A Facile Route for Patterned Growth of Metal–Insulator Carbon Lateral Junction through One-Pot Synthesis

Beomjin Park,[†,+] Jaesung Park,[‡,§,∥,+] Jin Gyeong Son,[⊥,▽,#] Yong-Jin Kim,[‡,§] Seong Uk Yu,[○,×] Hyo Ju Park,[⊗] Dong-Hun Chae,[∥] Jinseok Byun,[†] Gumhye Jeon,[†] Sung Huh,[⊥,▽] Seoung-Ki Lee,[¶] Artem Mishchenko,[§] Seung Hyun,[†] Tae Geol Lee,[#] Sang Woo Han,[⊥,▽] Jong-Hyun Ahn,[¶] Zonghoon Lee,[⊗] Chanyong Hwang,[△] Konstantin S. Novoselov,[§] Kwang S. Kim,[*,×] Byung Hee Hong,[*,‡] and Jin Kon Kim[*,†]

[†]National Creative Research Initiative Centre for Smart Block Copolymers, Department of Chemical Engineering, Pohang University of Science and Technology, Pohang 790-784, Republic of Korea, [‡]Department of Chemistry, College of Natural Sciences, Seoul National University, Seoul 151-747, Republic of Korea, [§]School of Physics and Astronomy, University of Manchester, Manchester M13 9PL, United Kingdom, [∥]Center for Electricity & Magnetism, Korea Research Institute of Standards and Science, Daejeon 305-340, Republic of Korea, [⊥]Department of Chemistry and KI for the NanoCentury, KAIST, Daejeon 305-701, Korea, [▽]Centre for Nanomaterials and Chemical Reactions, Institute for Basic Science (IBS), Daejeon 305-701, Republic of Korea, [#]Center for Nanosafety Metrology, Korea Research Institute of Standards and Science, Daejeon 305-340, Republic of Korea, [○]Department of Chemistry, Pohang University of Science and Technology, Pohang 790-784, Republic of Korea, [×]Department of Chemistry, Ulsan National Institute of Science and Technology (UNIST), Ulsan 689-798, Republic of Korea, [⊗]School of Materials Science and Engineering, Ulsan National Institute of Science and Technology (UNIST), Ulsan 689-798, Republic of Korea, [¶]School of Electrical and Electronic Engineering, Yonsei University, Seoul 120-749, Republic of Korea, and [△]Center for Nanometrology, Korea Research Institute of Standards and Science, Daejeon 305-340, Republic of Korea. [+]These authors contributed equally.

ABSTRACT Precise graphene patterning is of critical importance for tailor-made and sophisticated two-dimensional nanoelectronic and optical devices. However, graphene-based heterostructures have been grown by delicate multistep chemical vapor deposition methods, limiting preparation of versatile heterostructures. Here, we report one-pot synthesis of graphene/amorphous carbon (a-C) heterostructures from a solid source of polystyrene *via* selective photo-cross-linking process. Graphene is successfully grown from neat polystyrene regions, while patterned cross-linked polystyrene regions turn into a-C because of a large difference in their thermal stability. Since the electrical resistance of a-C is at least 2 orders of magnitude higher than that for graphene, the charge transport in graphene/a-C heterostructure occurs through the graphene region. Measurement of the quantum Hall effect in graphene/a-C lateral heterostructures clearly confirms the reliable quality of graphene and well-defined graphene/a-C interface. The direct synthesis of patterned graphene from polymer pattern could be further exploited to prepare versatile heterostructures.

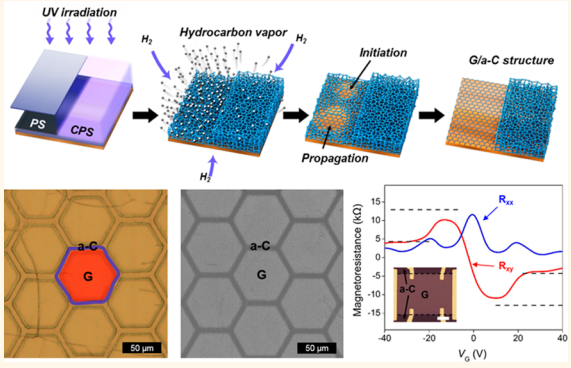

KEYWORDS: graphene · amorphous carbon · graphene-based heterostructure · bottom-up growth · graphene growth from polymer

Since graphene was first obtained by mechanical peeling method in 2004,[1] it has been extensively studied as a promising candidate for electronic devices,[2] owing to its exceptional electronic,[3,4] mechanical[5,6] and optical properties.[7] In wide-area applications, intricate patterning process for development of the micro (or nano) structured graphene is essential; however, common patterning methods require several steps such as lithographic techniques and wild etching process, resulting in damages and poor quality of graphene.[8−11]

To avoid these damages on graphene, many efforts have been introduced to grow the directly patterned graphene based on chemical vapor deposition (CVD) growth process.[12−16] For instance, inorganic materials with high temperature stability such as Al_2O_3 are used as an effective barrier for graphene growth.[14] This approach, however, requires delicate lithographic technique for barrier-positioning step before the growth of graphene and a removal step of the barrier to isolate the graphene for device application. Park and co-workers[12] used hexagonal boron nitride (h-BN) as

* Address correspondence to jkkim@postech.ac.kr, byunghee@snu.ac.kr, kimks@unist.ac.kr.

Received for review May 19, 2015 and accepted July 4, 2015.

Published online July 04, 2015
10.1021/acsnano.5b03037

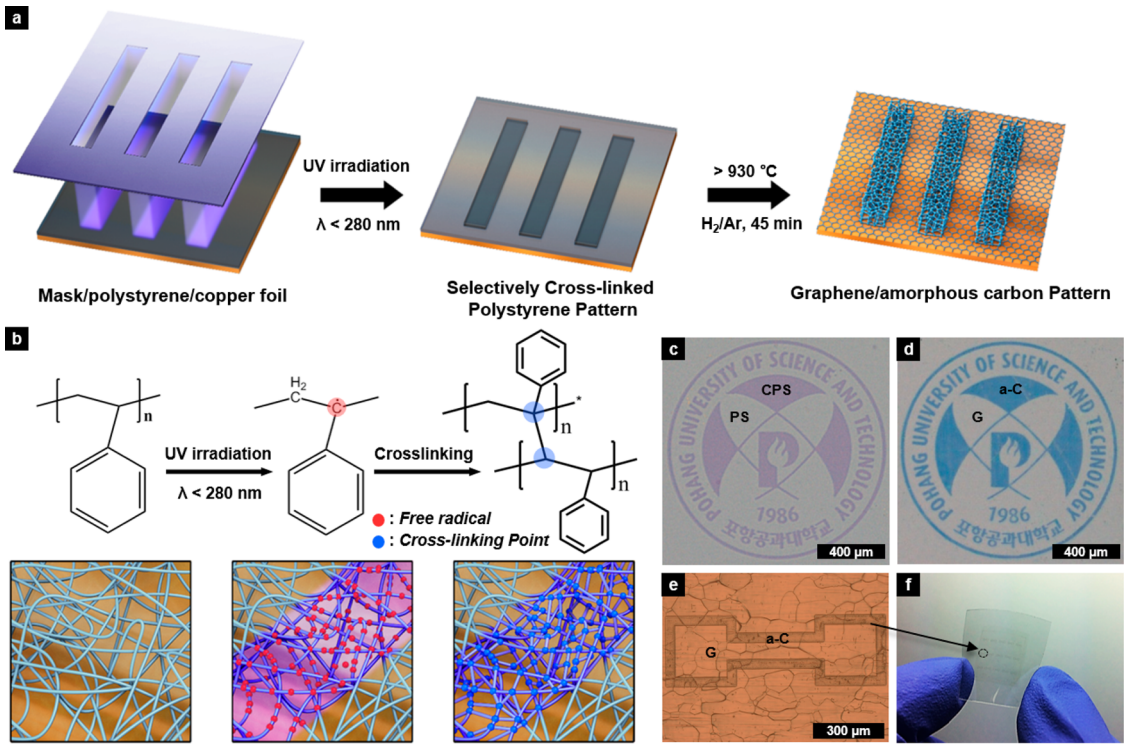

Figure 1. (a) Illustration of the fabrication procedure for graphene/a-C heterostructures from a solid source of polystyrene *via* control of its chemical structure. (b) Cross-linking mechanism of polystyrene by UV light. (c) Optical image of controlled cross-linked pattern of polystyrene. Light purple regions are neat PS, and the others are CPS. (d) Optical image of graphene/a-C transferred on SiO_2 (300 nm)/Si wafer. (e) Optical image of as-grown graphene device isolated by a-C. (f) Flexible device of graphene surrounded by a-C.

both an effective barrier for graphene growth and excellent electrical insulator. In this situation, even though the removal step of h-BN is not needed, this approach also requires three complicated steps: growth of the barrier in CVD, the removal of the unwanted region by lithography technique, and re-growth of graphene in CVD. On the other hand, the introduction of prepatterned seeds on copper foil allows to control the nucleation of graphene in CVD.[16,17] Although it gives the controlled single grain graphene with hexagon shape, the sophisticated control of various shapes, such as lines, squares, or dots, could not be impossible. Thus, there still remains a great challenge to find direct growth method for patterned graphene without damaging excellent properties of graphene.

Recent attempts to synthesize graphene from solid-phase carbon sources such as sucrose and poly(methyl methacrylate) suggest a new possibility for controllable growth of graphene.[18] For example, graphene grown from solid carbon source has been easily optimized to control doping level by employing polymers having nitrogen and boron atoms.[18,19] Furthermore, nano/micropatterned solid carbon source is expected to directly convert into patterned graphene. An easy way to achieve this pattern is that the polymer film is simply etched by using a lithographic mask, and the etched regions are directly open to the substrate. The solid carbon source at unetched regions indirectly converts into graphene through the hydrocarbon vapors formed from polymeric decomposition, such as CH_3 radicals.[20] However, because these hydrocarbon vapors are diffused on the etched regions, a physically patterned polymer film could not convert to patterned graphene.

Here, we developed a facile route for patterned growth of graphene/amorphous carbon lateral junction through one-pot synthesis. For this purpose, we first prepared a pattern consisting of polystyrene (PS) and cross-linked PS (CPS) regions by UV irradiation under vacuum on a patterned mask. In this situation, there is no empty region in the substrate which is directly exposed to air. When the PS film is exposed directly on UV, this region becomes CPS regions. CPS undergoes minimal decomposition into hydrocarbon vapors due to its high thermal stability, and so it simply converts into amorphous carbon (a-C) at high temperatures, while neat PS regions become graphene. In this way, CVD growth of the graphene/a-C heterostructure using cross-linking-driven chemical patterning of a solid carbon source of PS is achieved. Flexible devices fabricated from the graphene/a-C heterostructure show high mobility and excellent mechanical stability against bending.

RESULTS AND DISCUSSION

Figure 1a shows a schematic for the growth of the graphene/a-C heterostructure from the PS film. First,

copper foil is preannealed at 1000 °C for 30 min under a flow of 10 sccm hydrogen to remove the oxidized copper layer and organic impurities. Then, a 70 nm thick PS film is spin-coated on the as-annealed copper foil. This PS film is selectively exposed to UV light using a shielding mask for patterned growth. The a-C forms on the UV cured region of CPS chains, while graphene grows on the non-UV cured region. UV irradiation generates multiple radicals in the PS backbone chains through the oxidation process (Figure 1b). Each radical can form a new carbon−carbon bond with its nearest neighbor, thereby creating densely cross-linked networks.[21] A period of 12 h of UV radiation is required to obtain a uniform patterned CPS film on the substrate (Supporting Information Figure S1). Optical microscopy (OM) of microsized PS/CPS patterns on a SiO_2 (300 nm)/Si wafer shows two distinct regions of PS and CPS (Figure 1c). These regions are visible to the naked eye. In contrast with the conventional CVD growth from a gas carbon source,[22] the location of copper foil should be separated from the heating location, because PS decomposes at ~420 °C, which is much lower than the catalytic activation temperature of copper (higher than 950 °C; Supporting Information Figures S2 and S3). The as-prepared PS/CPS pattern on the copper foil converts to the graphene/a-C structure at 1050 °C, where graphene and a-C are selectively grown on PS and CPS regions, respectively (Figure 1d). The as-grown graphene/a-C heterostructure is successfully transferred to both rigid (SiO_2 (300 nm)/Si wafer) and flexible substrates (polyethylene terephthalate (PET)) using the poly(methyl methacrylate) (PMMA)-mediated transfer method[23] (Figure 1d−f). After removal of the PMMA support with acetone, wrinkle and PMMA residue are also observed on the graphene/a-C heterostructure, as shown in the atomic force microscopy (AFM, Supporting Information Figure S4), which is comparable with CVD graphene.[24] Graphene and a-C regions show transmittance of 97.7% and 96.1% at 550 nm, respectively. These transmittance measurements show that graphene consists mostly of monolayers[25] and the graphene/a-C heterostructure is transparent (Supporting Information Figure S5).

To investigate the growth mechanism of graphene/a-C heterostructures, the intermediate growth states in both regions are examined by scanning electron microscope (SEM) as a function of growth time. For a short growth time, up to 15 min, very thin PS-converted amorphous carbon films (a-C_{PS}) of 3 nm thickness appear due to extremely rapid heating (Figure 2a:1, Supporting Information Figure S6a). Some of this a-C_{PS} decomposes into hydrocarbon vapor due to the reaction between the carbon and hydrogen gas.[19] As this reaction proceeds, some regions on the copper foil are no longer covered with a-C_{PS}, and become nucleation sites for graphene growth, which results in partially grown graphene surrounded by a-C_{PS} after 30 min (Figure 2a:2). After 45 min, the graphene film fully covers the PS patterned area on the copper film (Figure 2a:3). CPS also converts into relatively thick a-C films (a-C_{CPS}), 10 nm thickness in 15 min (Supporting Information Figure S6b), and this region shows no visible change on the surface even after 45 min (Figure 2a:4−6). These observations concur with those obtained from thermogravimetric analysis (TGA), where PS completely decomposes above 420 °C, while CPS shows very slow decomposition even at 1050 °C due to its dense structure formed by bonding between PS chains (Figure 2b).

Even though both a-C_{PS} and a-C_{CPS} show almost identical Raman spectra (Supporting Information Figure S7), distinct differences for the samples are observed in time-of-flight secondary ion mass spectroscopy (ToF-SIMS) (Figure 2c). It is noted that a-C_{PS} produces much larger amount of carbon cluster ions than a-C_{CPS}, which indicates that the remaining a-C_{CPS} hardly converts into hydrocarbon vapor. Therefore, a-C_{CPS} acts as an effective barrier for graphene growth by preventing the penetration of hydrocarbon vapor onto the copper catalytic surface (Figure 2d). Additionally, the C_2 (m/z = 24) repeating units are observed more often in the spectra of a-C_{PS} than in those of a-C_{CPS}, indicating that a-C_{PS} can produce carbon dimers abundantly. Interestingly, these carbon dimers are known to be the intermediates to form graphene[26] and fullerene.[27] Thus, a-C_{PS} becomes a very effective carbon source for graphene growth, while a-C_{CPS} does not.

Figure 3a shows the OM image of as-grown graphene/a-C heterostructures on a copper foil, where red-labeled and blue-labeled regions are graphene and a-C, respectively. (It is noted that this hexagonal pattern does not indicate the hexagonal lattice of graphene). After transferring graphene/a-C heterostructures on a SiO_2/Si substrate, two regions (graphene and a-C) are clearly distinguishable in OM and scanning electron microscope (SEM) images (Figure 3b,c). To ensure whether graphene/a-C heterostructure is evenly grown, we utilize the different affinities between graphene and a-C. While graphene has sophisticated hexagonal lattice of carbon, a-C shows complex structure composed of sp^2 and sp^3 carbons. As polycyclic aromatic hydrocarbon, such as pentacene, is deposited on graphene/a-C heterostructure; pentacene thin films on graphene would favor a face-on orientation, while pentacene thin films on a-C would prefer an edge-on orientation.[24] Dark-field OM image shows light blue hexagons surrounded by dark hexagonal outlines, confirming that the graphene region and a-C region are uniformly grown in their own regions, respectively (Figure 3d, Supporting Information Figure S8).

To characterize the quality and uniformity of graphene/a-C heterostructure on SiO_2 (300 nm)/Si

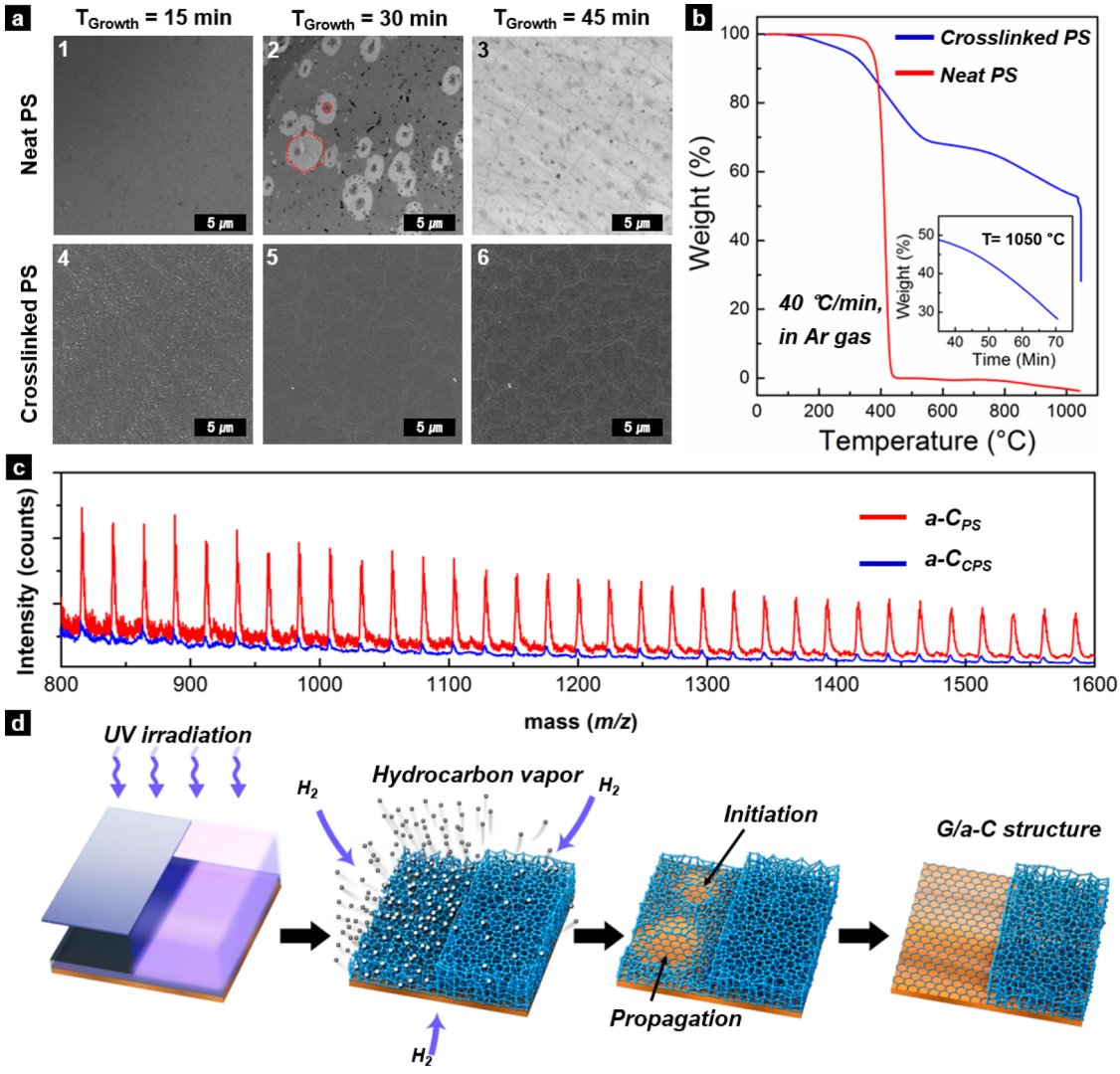

Figure 2. (a) SEM images showing the morphology change of neat PS and CPS depending on growth time. (b) TGA profiles of neat PS and CPS from room temperature to 1050 °C. While heating rate could be constantly maintained with 40 °C/min until 900 °C, the rate is highly reduced up to 5 °C/min after 900 °C. The inset is TGA profile *versus* time of CPS at 1050 °C. (c) Time-of-flight secondary ion mass spectroscopy (ToF-SIMS) data of a-C_{PS} and a-C_{CPS}. (d) Illustration of growth mechanism for graphene/a-C heterostructures.

substrate, Raman spectroscopy is carried out at a wavelength of 532 nm. The Raman spectra of graphene in graphene/a-C heterostructures is almost the same as those of pristine graphene (Figure 3e).[28] Because the absence of D band peak near 1350 cm^{-1} is one of the most salient features of defect-free graphene, D band peak is quantified as the ratio of D band peak intensity (I_D) and G band peak intensity (I_G), resulting in I_D/I_G of 0.05 from Figure 3e. Also, as the full width at half-maximum of 2D band peak ($fwhm_{2D}$) is another feature of defect-free graphene, $fwhm_{2D}$ is evaluated as 33 cm^{-1}, confirming the high quality of graphene.[29] Raman mapping image based on the Raman frequency of G (ω_G) and 2D (ω_{2D}) illustrates that the graphene/a-C heterostructures are uniform throughout the entire area (Figure 3f,g; Raman map of large-scale graphene/a-C is illustrated in Supporting Information Figure S9). From Raman maps of ω_G and ω_{2D}, G band peak and 2D band peak are statically observed at 1586.55 ± 0.31 and 2677.98 ± 0.18 cm^{-1}, respectively. According to Raman frequency of G and 2D band peaks, the resultant graphene in the heterostructure reveals a hole density of 4×10^{12} cm^{-2} and in-plane strain of 0.07%.[30] On the other hand, a-C shows an I_D/I_G of ~1.02 and a broad G band peak width of 80 cm^{-1}, indicating that the graphitic cluster size of a-C is smaller than 10 Å.[31,32] Also, from the peak position and the width of G band peak, and the ratio of integrated area of D to G band peak, the sp^3 fraction of a-C was roughly estimated to be 30−40%.[32] Thus, to determine a more exact value of the sp^3 fraction of a-C, we used X-ray photoelectron spectroscopy (XPS). From the area ratio at sp^2 and sp^3 peaks corresponding to 283.8 and 284.5 eV, respectively, the fraction of sp^3 is 25% (Supporting Information Figure S10).

In Figure 3h, the high resolution tunneling electron microscope (TEM) image and digital diffractogram

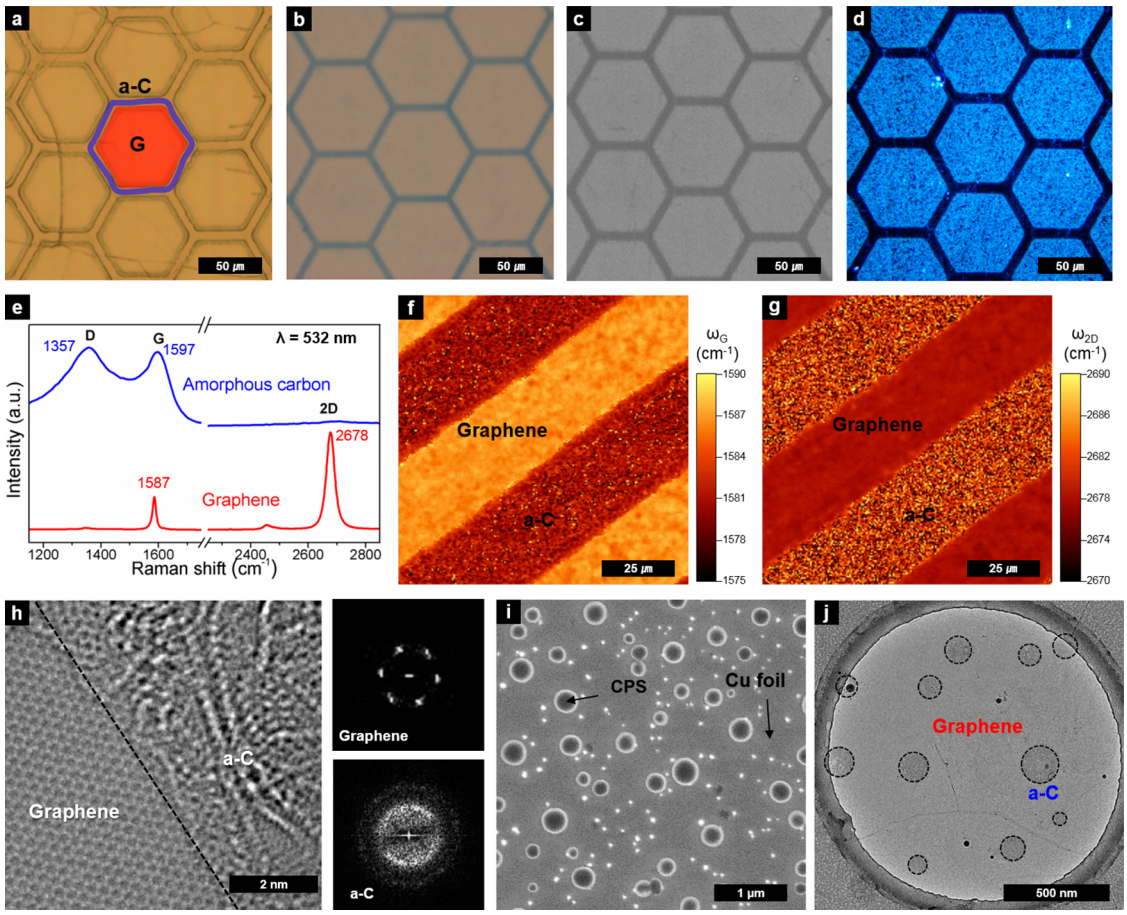

Figure 3. (a) OM image of as-grown graphene/a-C hexagonal pattern on copper foil. The six sides of hexagons are a-C, and the others are graphene. (b–d) OM image, SEM image and dark field OM image of graphene/a-C hexagonal pattern transfer to SiO_2/Si wafer. (e) Raman spectra from graphene and a-C. (f and g) Raman maps of graphene/a-C line pattern based on the Raman frequency of ω_G and ω_{2D}. (h) HR-TEM images and digital diffractograms of graphene and a-C. (i) SEM image of CPS islands on Cu foil. (j) Low magnification TEM image of a-C dots (dashed circles) surrounded by graphene.

reveal the structure of interface between graphene and a-C. Atomic resolution image in left panel directly displays that the left side is graphene region with hexagonal lattice feature, while the right side is randomly oriented amorphous carbon region. The digital diffractogram of graphene shows hexagonally packed spots with a spacing of 2.13 Å,[33,34] while that of a-C exhibits a ring pattern with the same spacing as graphene, indicating a noncrystalline structure. Though this result shows well-defined interface of graphene/a-C heterostructure at atomic resolution, photolithographic mask with a tolerance of ~150 nm induced a relatively broad boundary of graphene/a-C heterostructure. To demonstrate a sharp boundary as well as nanoscale pattern size, we used an immiscible PS/PMMA blend system, and showed a very sharp boundary between the graphene and a-C regions (Figure 3i,j, Supporting Information Figure S11 and S12). From these results, when the most-sophisticated lithographic mask for fabricating semiconductor integrated chips is used, a very small size pattern (sub-20 nm) with a sharp boundary would be realized.

We measure the electrical properties of the graphene/a-C heterostructures by fabricating field-effect transistor (FETs) devices. To reduce charged impurities (such as electron–hole puddle) on SiO_2, we prepared a self-assembled layer of hexamethyldisilazane (HMDS) on SiO_2(300 nm)/Si wafer.[35] Figure 4a shows two transfer curves for the stripe patterns of graphene/a-C heterostructure: the red curve is obtained from a graphene/a-C device with current flowing perpendicular to the stripes, and the blue curve is from another with current flowing parallel to the stripes. While the parallel device shows typical ambipolar behavior, the perpendicular device shows two-orders lower conductivity due to the relative insulating behavior of a-C (Supporting Information Figure S13). From this result, we conclude that the charge transport in the graphene/a-C heterostructure occurs through only the graphene region. Furthermore, from graphene/a-C FET measurement (red curve) as shown in Figure 4a, the hole density was 1.43×10^{12} cm^{-2}, which is different from that (4×10^{12} cm^{-2}) obtained by Raman analysis. The difference between two values arises because a quantitative analysis based on the Raman

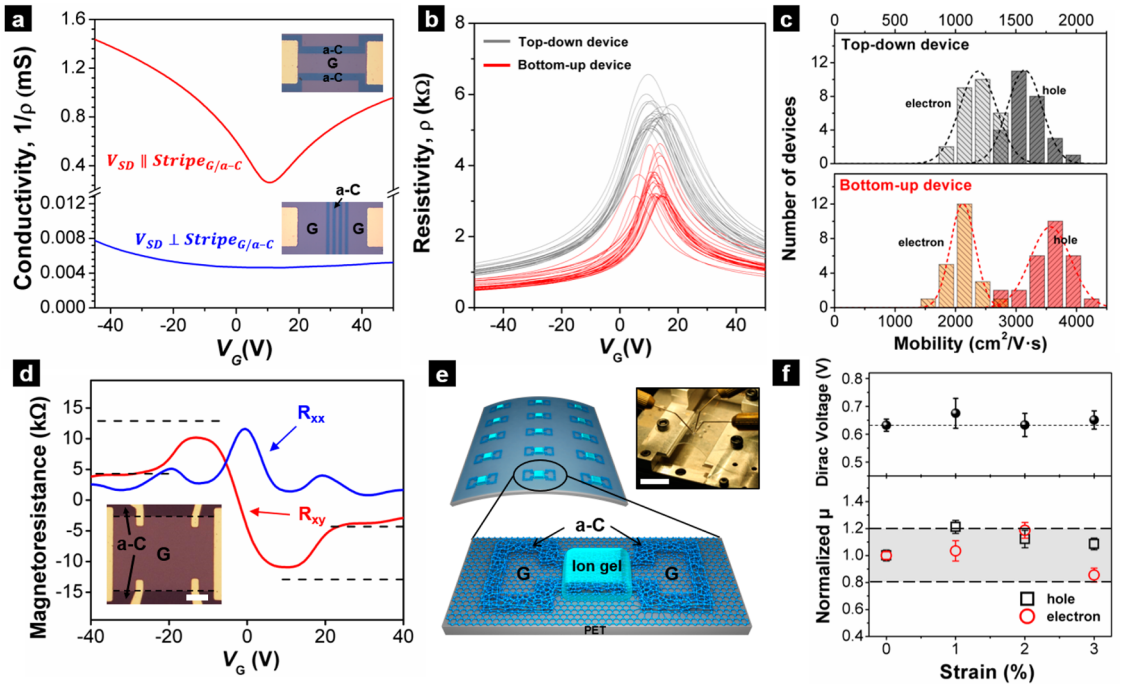

Figure 4. (a) Electrical measurements of graphene/a-C stripe pattern ($Stripe_{G/a-C}$): a graphene/a-C device with current flowing parallel to the stripes (red curve) and another with current flowing perpendicular to the stripes (blue curve). (b) Transfer characteristics of graphene FETs on 300 nm thick SiO_2/Si substrates: graphene-based top-down device (gray curves) and graphene/a-C heterostructure-based bottom-up device (red curves). (c) Probability distribution of charge carrier mobility for top-down device (upper panel) and bottom-up device (lower panel). (d) Electrical properties of graphene/a-C Hall bar device showing the half-integer quantum Hall effect. The inset shows the four-probe electrical resistance measurement graphene/a-C Hall bar device. Scale bar, 5 μm. (e) Illustration of flexible FET based on graphene/a-C heterostructure for bending test (left) and optical image of flexible graphene FET during bending test. Scale bar, 1 cm (right). (f) Plot of Dirac voltage (upper panel) and normalized mobility (lower panel) of hole and electron *versus* strain.

spectrum has been shown to be less reliable for CVD graphene of complex structure than exfoliated graphene. To compare a bottom-up process with a top-down process, we fabricated two types of devices (Figure 4b): a top-down device (gray curves) using graphene isolated by patterning process through lithography and plasma treatment, and a bottom-up device (red curves) using graphene inherently isolated by a-C without patterning process. To minimize the difference in graphene quality, graphene used in top-down device is identical to that used in bottom-up device. The electron/hole mobility (μ) of graphene device is determined by the equation $\mu = ((1/e)(\delta\sigma/\delta n))$, where e is elementary charge, σ is electrical conductivity, and n is gate dependent charge density.[36] As shown in Figure 4b,c, bottom-up device shows higher mobility (3570 $cm^2\ V^{-1}\ s^{-1}$ for hole) compared with top-down device (1590 $cm^2\ V^{-1}\ s^{-1}$ for hole). This result is consistent with common sense, that is, extra patterning processes using lithography and plasma treatment for top-down device fabrication could give damages on graphene surface, resulting in reduction of graphene quality.[37,38] The bottom-up device using graphene/a-C heterostructure shows better performance than the top-down device, even though the resistivity between graphene and a-C is not large enough (two-orders of magnitude difference). It is noted, however, that the resistivity of a-C is significantly increased with the decrease in growth temperature because of its temperature-dependent phase transition from nanocrystalline carbon network to amorphous carbon.[39] Furthermore, high quality graphene could be synthesized even at 500 °C, when the alloy catalyst of Au−Ni was used.[40] Thus, one can grow simultaneously both a-C with much higher resistance (at least four-orders of magnitude or above than graphene) and graphene maintaining high quality with a proper choice of alloy catalyst at optimized growth temperature.

The quantum Hall effect (QHE) of graphene is demonstrated by measuring the resistance *versus* gate bias at a low temperature (4 K) and a high magnetic field (15 T) (Figure 4d). Unlike conventional fabrication of graphene Hall bars on SiO_2 (300 nm)/Si substrate using lithographical techniques, in this study the electrodes were directly fabricated on the stripe-typed alternating graphene/a-C heterostructure film without plasma etching process to isolate the device channel area. We observe the half-integer QHE, as a fingerprint of single-layer graphene, with plateaus at filling factors $v = 2, 4$ at $R_{xy} = 1/2$ and $1/6\ (e^2/h)^{-1}$ (Here, R_{xx}/R_{xy} is longitudinal/transverse magnetoresistance; e is the elementary charge and h is Planck's constant). The sequence of plateaus for both electron and hole sides shows the existence of edge states in the structure,

indicating that the intrinsic property of graphene is well maintained in the graphene/a-C heterostructure-based Hall device. The slight mismatch with fully quantized values in both sides also exists. Furthermore, weak localization and activation energy with variation in temperature were also measured (Supporting Information Figures S14 and S15). The resultant electrical properties reveal the behavior of exfoliated and CVD graphene with several types of defects.[16,41−44]

To investigate the mechanical flexibility of the graphene/a-C heterostructure, we fabricate ion gel-gated graphene FETs surrounded by a-C on a PET substrate and measure the electrical performance under bending conditions as shown in Figure 4e (channel width 100 μm and length 550 μm).[45] Dirac voltage and hole/electron mobility are measured as a function of strain for the FETs. For a bending radius up to 8 mm, corresponding to a tensile strain value of 3%, both Dirac voltage and mobility are comparable to those of unstrained graphene (Figure 4f, Supporting Information Figure S16 and Table S1).[46] It should be noted that the interface between graphene and a-C gives little effect on the electrical property of heterostructure, which is indicative of an excellent mechanical stability at the interface. In addition, deformation such as local buckle, slip, or delamination of graphene from the substrate is not observed under repeated bending.

CONCLUSION

In summary, we show that the direct patterned growth of graphene from polymer patterns is a simple and innovative method to grow graphene-based heterostructures. Since CPS reveals higher thermal stability than PS, CPS converts into a-C which acts as an effective barrier preventing graphene growth, while PS converts into high quality patterned graphene. Importantly, the half-integer QHE observed in graphene/a-C lateral heterostructures clearly confirms the reliable quality of graphene and well-defined graphene/a-C interface. Also, the device performance of graphene is well maintained even at a strain of 3%, toward practical two-dimensional flexible electronics and optics. Furthermore, the heterostructures fabricated in this study could be easily extended to nanoscale patterned graphene once templates with nanosized patterns (for instance, block copolymers) are used.

METHODS

Preparation of Graphene/a-C Heterostructure. Copper foil (25 μm, 99.999%, Alfa Aesar) was thermally treated under a hydrogen vapor at 1000 °C for 15 min to remove metal oxide layers and organic impurities. Then, 2 wt % PS with a molecular weight (M_w) of 190 000 (Scientific Polymer Products) in chlorobenzene solution was spin-coated on the thermally treated copper foil at 2000 rpm for 20 s. The resultant PS film was baked at 30 min at 100 °C to remove the solvent, and the thickness of PS film was 70 nm. Selective cross-linking was made by UV irradiation (model G15T8, Sankyo Denki, Japan) of the sample under vacuum for 12 h, leading to a patterned PS film. Finally, the sample was annealed at 1050 °C under 1 Torr of Ar/H_2 atmosphere for 45 min, which converted it into the graphene/a-C heterostructure.

Molecular Orientation Control of Pentacene on Graphene/a-C. Graphene/a-C heterostructures were transferred onto a quartz substrate using the PMMA-mediated (M_w of 120 000: Aldrich Chemical Co.) transfer method. The PMMA support is removed with acetone. To remove the remaining PMMA residues, this sample was annealed at 500 °C for 30 min under an Ar/H_2 atmosphere. Then, pentacene (Aldrich Chemicals, no purification) with a thickness of 50 nm was thermally evaporated onto the resulting graphene/a-C heterostructures at a rate of 0.2 Å/s.

Characterization of Graphene/a-C Heterostructure. The morphologies of graphene/a-C heterostructures were investigated by OM (Ziess) and field-emission SEM (Hitachi, S4800). The Raman spectra and mapping were performed utilizing confocal Raman spectroscopy (WITec) with a 532 nm excitation laser. Aberration-corrected FEI Titan Cube TEM (FEI Titan3 G2 60-300) operating at 80 kV was employed to observe the interface of the graphene/a-C heterostructure and obtain the digital diffractogram. The thermal stability of PS and CPS was analyzed by TGA (TA Instruments, Q600) at a rate of 40 °C/min under Ar atmosphere. ToF-SIMS measurements of films surfaces were taken using a TOF-SIMS V (ION-TOF GmbH, Germany). Argon cluster primary ions (Ar_{1000}^+) at 20 kV and a repetition rate of 6.6 kHz with an incident angle of 45° to the surface normal were used to obtain positive spectra. The analysis area of 200 × 200 μm^2 was randomly rastered by the primary ions, and the primary ion dose was maintained below 10^{12} ions/cm^2 to ensure static SIMS conditions. The mass resolution ($M/\Delta M$) at m/z 800 was higher than 1000, and the positive ion spectra were internally calibrated using CH_3^+, $C_2H_3^+$, and $C_3H_5^+$. The morphologies of the pentacene film were measured by AFM (Digital Instrument) with tapping mode. The fluorescence images and spectra of pentacene were characterized by fluorescence OM (Olympus, FV1000). To study the molecular orientation of pentacene, 2D grazing incidence X-ray diffraction (GIXD) experiments were performed at the 3C and 9A beamlines of the Pohang Accelerator Laboratory.

Measurement of Graphene/a-C Heterostructure-Based FET Devices. To operate the flexible graphene transistor, a UV-patternable electrolyte was employed as a gate dielectric. First, the UV-cross-linkable ion gel ink, which is composed of 1-ethyl-3-methylimidazolium bis(trifluoromethylsulfonyl)imide ([EMIM][TFSI] ionic liquid, poly(ethylene glycol) diacrylate (PEG-DA) monomer, and 2-hydroxy-2-methylpropiophenone (HOMPP) initiator (weight ratio of 81:6:3), was spin-cast on the channel region and exposed to UV light (100 mW/cm^2 at 365 nm) for 5 s to initiate polymerization. Next, poly(3,4-ethylenedioxythiophene) oxidized with poly(4-styrenesulfonate) was transferred to the top of the ion gel layer using polydimethylsiloxane to form a gate electrode. The specific capacitance of the ion gel was measured to be 7.29 μF/cm^2 at 10 Hz, much larger than typical values for 300 nm thick SiO_2 dielectrics (10.8 nF/cm^2).

Conflict of Interest: The authors declare no competing financial interest.

Supporting Information Available: Experimental details, variation of film thickness and degree of crosslinking as a function of UV exposure time, analysis of pentacene film grown on graphene and a-CCPS characterization by Raman, AFM, XPS, SEM, HR-TEM, and UV-Vis-NIR and transport properties (resistivity, magnetoconductivity, conductivity). The Supporting Information is available free of charge on the ACS Publications website at DOI: 10.1021/acsnano.5b03037.

Acknowledgment. We thank Hyun Jin Park (NINC) for TEM operation. This work was supported by National Creative Research Initiative Program (No. 2013R1A3A2042196), National

Honor Scientist Program (No. 2010-0020414), the Global Research Lab (GRL) Program (2011-0021972) and International Research & Development Program (No. 2012K1A3A7A03057505) of the National Research Foundation of Korea (NRF) funded by Korean government (MEST). This work was performed as part of EMRP project GraphOhm. The EMRP is jointly funded by the EMRP participating countries within EURAMET and the European Union.

REFERENCES AND NOTES

1. Novoselov, K. S.; Geim, A. K.; Morozov, S. V.; Jiang, D.; Zhang, Y.; Dubonos, S. V.; Grigorieva, I. V.; Firsov, A. A. Electric Field Effect in Atomically Thin Carbon Films. *Science* **2004**, *306*, 666–669.
2. Bonaccorso, F.; Sun, Z.; Hasan, T.; Ferrari, A. C. Graphene Photonics and Optoelectronics. *Nat. Photonics* **2010**, *4*, 611–622.
3. Novoselov, K. S.; Geim, A. K.; Morozov, S. V.; Jiang, D.; Katsnelson, M. I.; Grigorieva, I. V.; Dubonos, S. V.; Firsov, A. A. Two-Dimensional Gas of Massless Dirac Fermions in Graphene. *Nature* **2005**, *438*, 197–200.
4. Novoselov, K. S.; Jiang, Z.; Zhang, Y.; Morozov, S. V.; Stormer, H. L.; Zeitler, U.; Maan, J. C.; Boebinger, G. S.; Kim, P.; Geim, A. K. Room-Temperature Quantum Hall Effect in Graphene. *Science* **2007**, *315*, 1379–1379.
5. Lee, C.; Wei, X. D.; Kysar, J. W.; Hone, J. Measurement of the Elastic Properties and Intrinsic Strength of Monolayer Graphene. *Science* **2008**, *321*, 385–388.
6. Bae, S.; Kim, H.; Lee, Y.; Xu, X. F.; Park, J. S.; Zheng, Y.; Balakrishnan, J.; Lei, T.; Kim, H. R.; Song, Y. I.; et al. Roll-to-Roll Production of 30-Inch Graphene Films for Transparent Electrodes. *Nat. Nanotechnol.* **2010**, *5*, 574–578.
7. Bao, Q. L.; Zhang, H.; Wang, B.; Ni, Z. H.; Lim, C. H. Y. X.; Wang, Y.; Tang, D. Y.; Loh, K. P. Broadband Graphene Polarizer. *Nat. Photonics* **2011**, *5*, 411–415.
8. Saloriutta, K.; Hancock, Y.; Karkkainen, A.; Karkkainen, L.; Puska, M. J.; Jauho, A. P. Electron Transport in Edge-Disordered Graphene Nanoribbons. *Phys. Rev. B: Condens. Matter Mater. Phys.* **2011**, *83*, 205125.
9. Sinitskii, A.; Tour, J. M. Patterning Graphene through the Self-Assembled Templates: Toward Periodic Two-Dimensional Graphene Nanostructures with Semiconductor Properties. *J. Am. Chem. Soc.* **2010**, *132*, 14730–14732.
10. Tour, J. M. Top-Down *Versus* Bottom-up Fabrication of Graphene-Based Electronics. *Chem. Mater.* **2014**, *26*, 163–171.
11. Wang, Y.; Xu, X. F.; Lu, J.; Lin, M.; Bao, Q. L.; Ozyilmaz, B.; Loh, K. P. Toward High Throughput Interconvertible Graphane-to-Graphene Growth and Patterning. *ACS Nano* **2010**, *4*, 6146–6152.
12. Levendorf, M. P.; Kim, C. J.; Brown, L.; Huang, P. Y.; Havener, R. W.; Muller, D. A.; Park, J. Graphene and Boron Nitride Lateral Heterostructures for Atomically Thin Circuitry. *Nature* **2012**, *488*, 627–632.
13. Liu, Z.; Ma, L. L.; Shi, G.; Zhou, W.; Gong, Y. J.; Lei, S. D.; Yang, X. B.; Zhang, J. N.; Yu, J. J.; Hackenberg, K. P.; et al. In-Plane Heterostructures of Graphene and Hexagonal Boron Nitride with Controlled Domain Sizes. *Nat. Nanotechnol.* **2013**, *8*, 119–124.
14. Safron, N. S.; Kim, M.; Gopalan, P.; Arnold, M. S. Barrier-Guided Growth of Micro- and Nano-Structured Graphene. *Adv. Mater.* **2012**, *24*, 1041–1045.
15. Gong, Y. J.; Shi, G.; Zhang, Z. H.; Zhou, W.; Jung, J.; Gao, W. L.; Ma, L. L.; Yang, Y.; Yang, S. B.; You, G.; et al. Direct Chemical Conversion of Graphene to Boron- and Nitrogen- and Carbon-Containing Atomic Layers. *Nat. Commun.* **2014**, *5*, 3193.
16. Yu, Q. K.; Jauregui, L. A.; Wu, W.; Colby, R.; Tian, J. F.; Su, Z. H.; Cao, H. L.; Liu, Z. H.; Pandey, D.; Wei, D. G.; et al. Control and Characterization of Individual Grains and Grain Boundaries in Graphene Grown by Chemical Vapour Deposition. *Nat. Mater.* **2011**, *10*, 443–449.
17. Wu, W.; Jauregui, L. A.; Su, Z. H.; Liu, Z. H.; Bao, J. M.; Chen, Y. P.; Yu, Q. K. Growth of Single Crystal Graphene Arrays by Locally Controlling Nucleation on Polycrystalline Cu Using Chemical Vapor Deposition. *Adv. Mater.* **2011**, *23*, 4898–4903.
18. Sun, Z. Z.; Yan, Z.; Yao, J.; Beitler, E.; Zhu, Y.; Tour, J. M. Growth of Graphene from Solid Carbon Sources. *Nature* **2010**, *468*, 549–552.
19. Ji, H. X.; Hao, Y. F.; Ren, Y. J.; Charlton, M.; Lee, W. H.; Wu, Q. Z.; Li, H. F.; Zhu, Y. W.; Wu, Y. P.; Piner, R.; et al. Graphene Growth Using a Solid Carbon Feedstock and Hydrogen. *ACS Nano* **2011**, *5*, 7656–7661.
20. Kwak, J.; Kwon, T. Y.; Chu, J. H.; Choi, J. K.; Lee, M. S.; Kim, S. Y.; Shin, H. J.; Park, K.; Park, J. U.; Kwon, S. Y. *In Situ* Observations of Gas Phase Dynamics During Graphene Growth Using Solid-State Carbon Sources. *Phys. Chem. Chem. Phys.* **2013**, *15*, 10446–10452.
21. Wells, R. K.; Royston, A.; Badyal, J. P. S. Direct Evidence for the Generation of Phenyl Radicals and Cross-Linking During the Photolysis of Polystyrene Film. *Macromolecules* **1994**, *27*, 7465–7468.
22. Kim, K. S.; Zhao, Y.; Jang, H.; Lee, S. Y.; Kim, J. M.; Kim, K. S.; Ahn, J. H.; Kim, P.; Choi, J. Y.; Hong, B. H. Large-Scale Pattern Growth of Graphene Films for Stretchable Transparent Electrodes. *Nature* **2009**, *457*, 706–710.
23. Reina, A.; Jia, X. T.; Ho, J.; Nezich, D.; Son, H. B.; Bulovic, V.; Dresselhaus, M. S.; Kong, J. Large Area, Few-Layer Graphene Films on Arbitrary Substrates by Chemical Vapor Deposition. *Nano Lett.* **2009**, *9*, 30–35.
24. Lee, W. H.; Park, J.; Sim, S. H.; Lim, S.; Kim, K. S.; Hong, B. H.; Cho, K. Surface-Directed Molecular Assembly of Pentacene on Monolayer Graphene for High-Performance Organic Transistors. *J. Am. Chem. Soc.* **2011**, *133*, 4447–4454.
25. Nair, R. R.; Blake, P.; Grigorenko, A. N.; Novoselov, K. S.; Booth, T. J.; Stauber, T.; Peres, N. M. R.; Geim, A. K. Fine Structure Constant Defines Visual Transparency of Graphene. *Science* **2008**, *320*, 1308–1308.
26. Niu, T. C.; Zhou, M.; Zhang, J. L.; Feng, Y. P.; Chen, W. Growth Intermediates for Cvd Graphene on Cu(111): Carbon Clusters and Defective Graphene. *J. Am. Chem. Soc.* **2013**, *135*, 8409–8414.
27. Kroto, H. W.; Heath, J. R.; O'Brien, S. C.; Curl, R. F.; Smalley, R. E. C60: Buckminsterfullerene. *Nature* **1985**, *318*, 162–163.
28. Ferrari, A. C.; Meyer, J. C.; Scardaci, V.; Casiraghi, C.; Lazzeri, M.; Mauri, F.; Piscanec, S.; Jiang, D.; Novoselov, K. S.; Roth, S.; et al. Raman Spectrum of Graphene and Graphene Layers. *Phys. Rev. Lett.* **2006**, *97*, 187401.
29. Li, X. S.; Cai, W. W.; An, J. H.; Kim, S.; Nah, J.; Yang, D. X.; Piner, R.; Velamakanni, A.; Jung, I.; Tutuc, E.; et al. Large-Area Synthesis of High-Quality and Uniform Graphene Films on Copper Foils. *Science* **2009**, *324*, 1312–1314.
30. Lee, J. E.; Ahn, G.; Shim, J.; Lee, Y. S.; Ryu, S. Optical Separation of Mechanical Strain from Charge Doping in Graphene. *Nat. Commun.* **2012**, *3*, 1024.
31. Schwan, J.; Ulrich, S.; Batori, V.; Ehrhardt, H.; Silva, S. R. P. Raman Spectroscopy on Amorphous Carbon Films. *J. Appl. Phys.* **1996**, *80*, 440–447.
32. Ferrari, A. C.; Robertson, J. Interpretation of Raman Spectra of Disordered and Amorphous Carbon. *Phys. Rev. B: Condens. Matter Mater. Phys.* **2000**, *61*, 14095–14107.
33. Meyer, J. C.; Geim, A. K.; Katsnelson, M. I.; Novoselov, K. S.; Booth, T. J.; Roth, S. The Structure of Suspended Graphene Sheets. *Nature* **2007**, *446*, 60–63.
34. Kim, K.; Lee, Z.; Regan, W.; Kisielowski, C.; Crommie, M. F.; Zettl, A. Grain Boundary Mapping in Polycrystalline Graphene. *ACS Nano* **2011**, *5*, 2142–2146.
35. Lafkioti, M.; Krauss, B.; Lohmann, T.; Zschieschang, U.; Klauk, H.; von Klitzing, K.; Smet, J. H. Graphene on a Hydrophobic Substrate: Doping Reduction and Hysteresis Suppression under Ambient Conditions. *Nano Lett.* **2010**, *10*, 1149–1153.
36. Das, A.; Pisana, S.; Chakraborty, B.; Piscanec, S.; Saha, S. K.; Waghmare, U. V.; Novoselov, K. S.; Krishnamurthy, H. R.; Geim, A. K.; Ferrari, A. C.; et al. Monitoring Dopants by Raman Scattering in an Electrochemically Top-Gated Graphene Transistor. *Nat. Nanotechnol.* **2008**, *3*, 210–215.
37. Fan, J. Y.; Michalik, J. M.; Casado, L.; Roddaro, S.; Ibarra, M. R.; De Teresa, J. M. Investigation of the Influence on Graphene

by Using Electron-Beam and Photo-Lithography. *Solid State Commun.* **2011**, *151*, 1574–1578.
38. Shen, X. N.; Wang, H. M.; Yu, T. How Do the Electron Beam Writing and Metal Deposition Affect the Properties of Graphene During Device Fabrication? *Nanoscale* **2013**, *5*, 3352–3358.
39. Turchanin, A.; Beyer, A.; Nottbohm, C. T.; Zhang, X. H.; Stosch, R.; Sologubenko, A.; Mayer, J.; Hinze, P.; Weimann, T.; Golzhauser, A. One Nanometer Thin Carbon Nanosheets with Tunable Conductivity and Stiffness. *Adv. Mater.* **2009**, *21*, 1233–1237.
40. Weatherup, R. S.; Bayer, B. C.; Blume, R.; Ducati, C.; Baehtz, C.; Schlogl, R.; Hofmann, S. *In Situ* Characterization of Alloy Catalysts for Low-Temperature Graphene Growth. *Nano Lett.* **2011**, *11*, 4154–4160.
41. Tikhonenko, F. V.; Horsell, D. W.; Gorbachev, R. V.; Savchenko, A. K. Weak Localization in Graphene Flakes. *Phys. Rev. Lett.* **2008**, *100*, 056802.
42. Baker, A. M. R.; Alexander-Webber, J. A.; Altebaeumer, T.; Janssen, T. J. B. M.; Tzalenchuk, A.; Lara-Avila, S.; Kubatkin, S.; Yakimova, R.; Lin, C. T.; Li, L. J.; et al. Weak Localization Scattering Lengths in Epitaxial, and Cvd Graphene. *Phys. Rev. B: Condens. Matter Mater. Phys.* **2012**, *86*, 235441.
43. Heo, J.; Chung, H. J.; Lee, S. H.; Yang, H.; Seo, D. H.; Shin, J. K.; Chung, U. I.; Seo, S.; Hwang, E. H.; Das Sarma, S. Nonmonotonic Temperature Dependent Transport in Graphene Grown by Chemical Vapor Deposition. *Phys. Rev. B: Condens. Matter Mater. Phys.* **2011**, *84*, 035421.
44. Song, H. S.; Li, S. L.; Miyazaki, H.; Sato, S.; Hayashi, K.; Yamada, A.; Yokoyama, N.; Tsukagoshi, K. Origin of the Relatively Low Transport Mobility of Graphene Grown through Chemical Vapor Deposition. *Sci. Rep.* **2012**, *2*, 337.
45. Lee, S. K.; Kim, B. J.; Jang, H.; Yoon, S. C.; Lee, C.; Hong, B. H.; Rogers, J. A.; Cho, J. H.; Ahn, J. H. Stretchable Graphene Transistors with Printed Dielectrics and Gate Electrodes. *Nano Lett.* **2011**, *11*, 4642–4646.
46. Suo, Z.; Ma, E. Y.; Gleskova, H.; Wagner, S. Mechanics of Rollable and Foldable Film-on-Foil Electronics. *Appl. Phys. Lett.* **1999**, *74*, 1177–1179.